Effect of the Microstructure of a *Hyperbranched* Polymer and Nanoclay Loading on the Morphology and Properties of Novel Polyurethane Nanocomposites

Pradip K. Maji, Prasanta K. Guchhait, and Anil K. Bhowmick*

Rubber Technology Centre, Indian Institute of Technology, Kharagpur 721302, India

ABSTRACT Novel polyurethane nanocomposites based on toluene diisocyanate, poly(propylene glycol), various hyperbranched polymers (HBPs), and layered silicate were synthesized with the aim of determining the effect of the layered silicate loading and the functionality of HBP on the structure and properties of polyurethane nanocomposites. The microstructure of the nanocomposites was investigated by X-ray diffraction analysis and high-resolution transmission electron microscopy. It was found that exfoliated morphology and good dispersion were obtained up to 8 phr clay loading for all of the nanocomposites. ~100% increment in tensile strength, ~2-fold increase in the lap shear strength, ~200% increment in the peel strength, and 120% increment in the storage modulus along with a dramatic improvement in thermal stability were observed with the addition of 8 phr clay, over the pristine polyurethane. The higher the level of functionality of the HBP, the higher is the property enhancement. These properties were correlated with the state of dispersion of the clay platelets in the polyurethane matrix, the structure of the matrix, and clay–polymer interaction.

KEYWORDS: polyurethane • nanocomposites • layered silicate • hyperbranched polymer

INTRODUCTION

Present day technology requires materials with unusual combinations of properties that cannot be met by the conventional classes of materials: metals, ceramics, and polymers. As a result, engineers and technologists are compelled to search for alternative materials to meet complex service requirements for today's applications, where the desired material properties are low density, high tensile strength, low- to high-temperature applicability, low gas permeability, and high abrasion and impact resistance. The combination and ranges of these contradicting material properties could be met by the development of special composites.

These novel materials can have expected properties arising from synergism of the components. In recent years, researches in organic–inorganic nanocomposites, particularly in the development of new polymer/clay-based nanocomposites, have become popular (1–4). Montmorillonite (MMT) is one of the most promising layered silicate clays used as the inorganic filler for the preparation of nanocomposites because of its high aspect ratio and natural abundance (5–7). Many polymer/clay nanocomposite materials such as polycaprolactone/organoclay (8), polystyrene/organoclay (9, 10), epoxy/organoclay (11–14), polyimide/organoclay (15, 16), fluoroelastomers/clay (17), poly[styrene-*b*-(ethylene-*co*-butylene)-*b*-styrene]/organoclay (18), styrene butadiene rubber/organoclay (19), and poly(methyl methacrylate)/organoclay (20–22) systems have been reported.

Polyurethanes (PUs) are unique polymeric materials with a wide range of physical and chemical properties. They have wide applications as space materials. Because many different monomers are now commercially available and tailor-made properties can be obtained from well-designed combinations of precursors, PUs can be tailored to meet the highly diversified demands of modern technologies such as coatings, adhesives, fiber, foams, and thermoplastic elastomers (23). Several papers published on this topic show that, by changing the composition and the conditions of processing, one can influence the chemical and morphological structures of PUs and their properties (24).

Various experiments aimed at improving both the thermal stability and mechanical properties of PUs have been conducted. One attempt to improve the physical properties and thermal stability of PUs involves chemical modification of their backbones by a highly stable heterocyclic group. Another modification involves the incorporation of an organically modified nanoclay to achieve nanocomposite formation (25–27). In general, because of the ultrafine phase dimensions, nanocomposites exhibit new and improved properties in comparison with their microcomposite and macrocomposite counterparts (28–34). For a true nanocomposite, the clay layer must be uniformly dispersed in the polymer matrix rather than aggregated as tactoids. Once good dispersion has been achieved, physical, thermal, mechanical, and adhesion properties are found to increase.

In the adaptation of clay nanocomposite technology to PUs, two main issues need to be addressed: (1) control of

* Corresponding author.E mail: anilkb@rtc.iitkgp.ernet.in. Phone: 91-3222-283180. Fax: 91-3222-220312.
Received for review August 26, 2008 and accepted October 06, 2008

DOI: 10.1021/am800020k

the degree of exfoliation; (2) comparability of the existing processing routes. In PU thermosets, isocyanate (−NCO)-functionalized prepolymers of oligomers are introduced via polyol. Hence, if the polyol is to be substituted by polyol/clay, the polymer must interact strongly with the clay. This has led to interest in the use of −OH-functionalized polyol materials. However, preliminary studies on the processing of PU prepolymers with polyol materials in the presence of an organically modified MMT clay have shown to provide a means of obtaining exfoliated nanocomposites without aggregation (35, 36).

Since the pioneering work of well-defined, three-dimensional structural, ordered macromolecules by Vögtle et al. (37), Tomalia et al. (38, 39), and Newkome et al. (40), interest in dendrimers and hyperbranched polymers (HBPs) has been increasing at an amazing rate. This is because of the presence of numerous end groups in these branched polymers for special purpose applications. Unique copolymers with core−shell architectures or a highly cross-linked network can be achieved via the incorporation of dendritic structures. Recent developments of synthetic procedures have made functionalized dendrimers readily available in large enough quantities to facilitate the rapid development of dendrimer chemistry.

However, polymerization of PU prepolymers with polyester HBPs in the presence of an organically modified MMT clay may provide a means of obtaining exfoliated nanocomposites without aggregation. Until now, there are only a few literature references (41, 42) on PUs having HBPs. A huge gap is also present in the literature references on PUs based on HBPs and their nanocomposites.

The present study has focused on the synthesis of new PU nanocomposites based on a hyperbranched polyester and the investigation of their morphology and mechanical, adhesion, and thermal properties and is also intended to provide a basis for assessing the nanofillers as additives in the practical PU formulations. Given that they are highly dependent on the amount of fillers, the properties are also expected to provide a sensitive measure of the degree of exfoliation. The focus of the study is on the structure−property relationship of new PU nanocomposites and their applicability as space materials.

EXPERIMENTAL SECTION

Materials. Poly(propylene glycol) (PPG), molecular weight 2000, was procured from Sigma-Aldrich Chemicals, Bangalore, India. Toluene 2,4-diisocyanate (TDI) was purchased from Merck Schuchardt OHG, Hohenbrunn, Germany. The reactive clay, Cloisite 30B contained 90 mequiv of quaternary ammonium ions/100 g of clay and was purchased from Southern Clay Products, Gonzales, TX. The quaternary ammonium ion has a structure of $N^+(CH_2CH_2OH)_2(CH_3)T$, with T representing an alkyl group of approximately 65% $C_{18}H_{37}$, 30% $C_{16}H_{33}$, and 5% $C_{14}H_{29}$. Dibutyltin dilaurate (DBTL) was procured from Aldrich Chemicals, Bangalore, India. Dry solvent, tetrahydrofuran (THF), was purchased from Rankem, Kolkata, India. Second-generation (H20), third-generation (H30), and fourth-generation (H40) hyperbranched polyesters were procured from Perstorp Specialty Chemicals AB, Perstorp, Sweden. The structures of the HBPs are shown in Figure 1. Characteristic properties are given in Table 1.

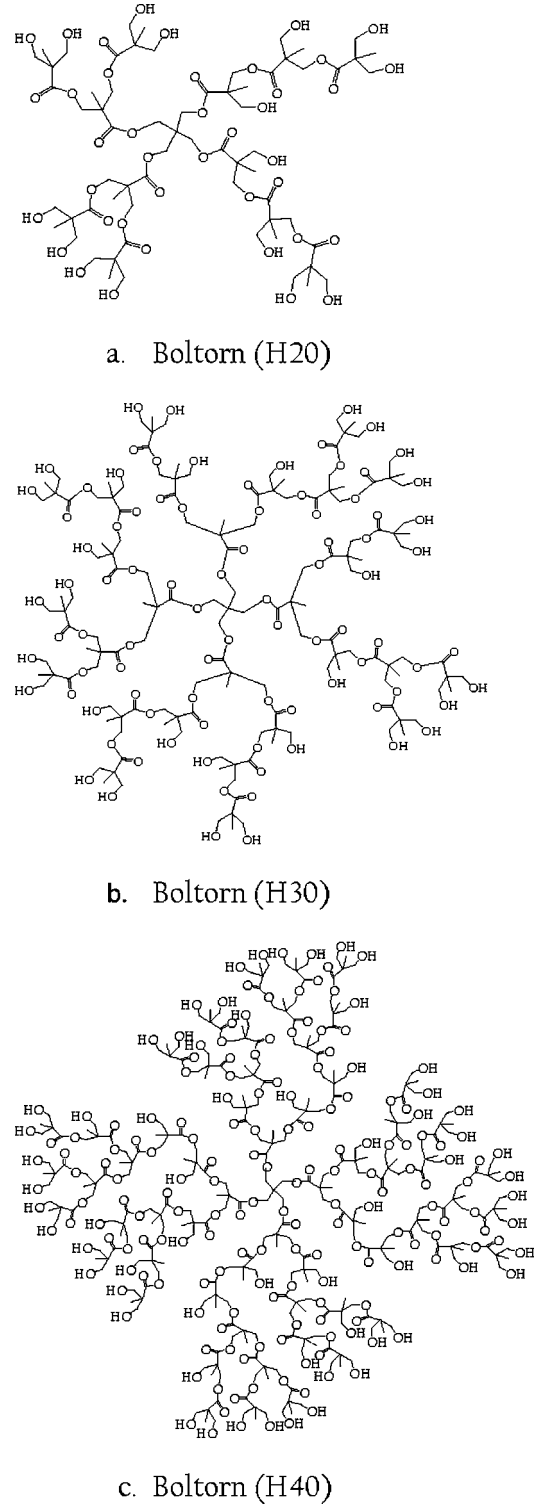

FIGURE 1. Structures of different HBPs: (a) second generation (H20); (b) third generation (H30); (c) fourth generation (H40).

Synthesis of the PU Prepolymer. The PU prepolymer was synthesized in a nitrogen atmosphere by reacting 2 mol of TDI with 1 mol of PPG at 80 °C in a round-bottomed flask (500 cm^3) with continuous stirring. The reaction scheme is given in Scheme 1. The exothermic reaction was controlled by cooling, and the temperature was maintained at 80 °C. The isocyanate (−NCO) concentration in the prepolymer reached a constant value after 4 h. The isocyanate content in the prepolymer was 4.4%, which was determined by the titrametric method. The viscosity of the prepolymer determined by ASTM part 22D-1084

Table 1. Characteristics of Hyperbranched Polyesters [Boltorn H*x* (*x* = 20, 30, 40)]

Boltorn H*x*	average no. of functional groups	$M_{theoretical}$ (g/mol)	M_w (g/mol) (by GPC)	M_w/M_n	hydroxyl number (mg of KOH/g)	acid number (mg of KOH/g)	T_g (°C)
H20	16	1748	2100	1.3	490−520	5−9	25
H30	32	3604	3500	1.5	480−510	6−10	35
H40	64	7316	5100	1.8	470−500	7−11	40

Scheme 1. Reaction Scheme of the Cross-Linking of a PU Prepolymer with Hyperbranched Polyol

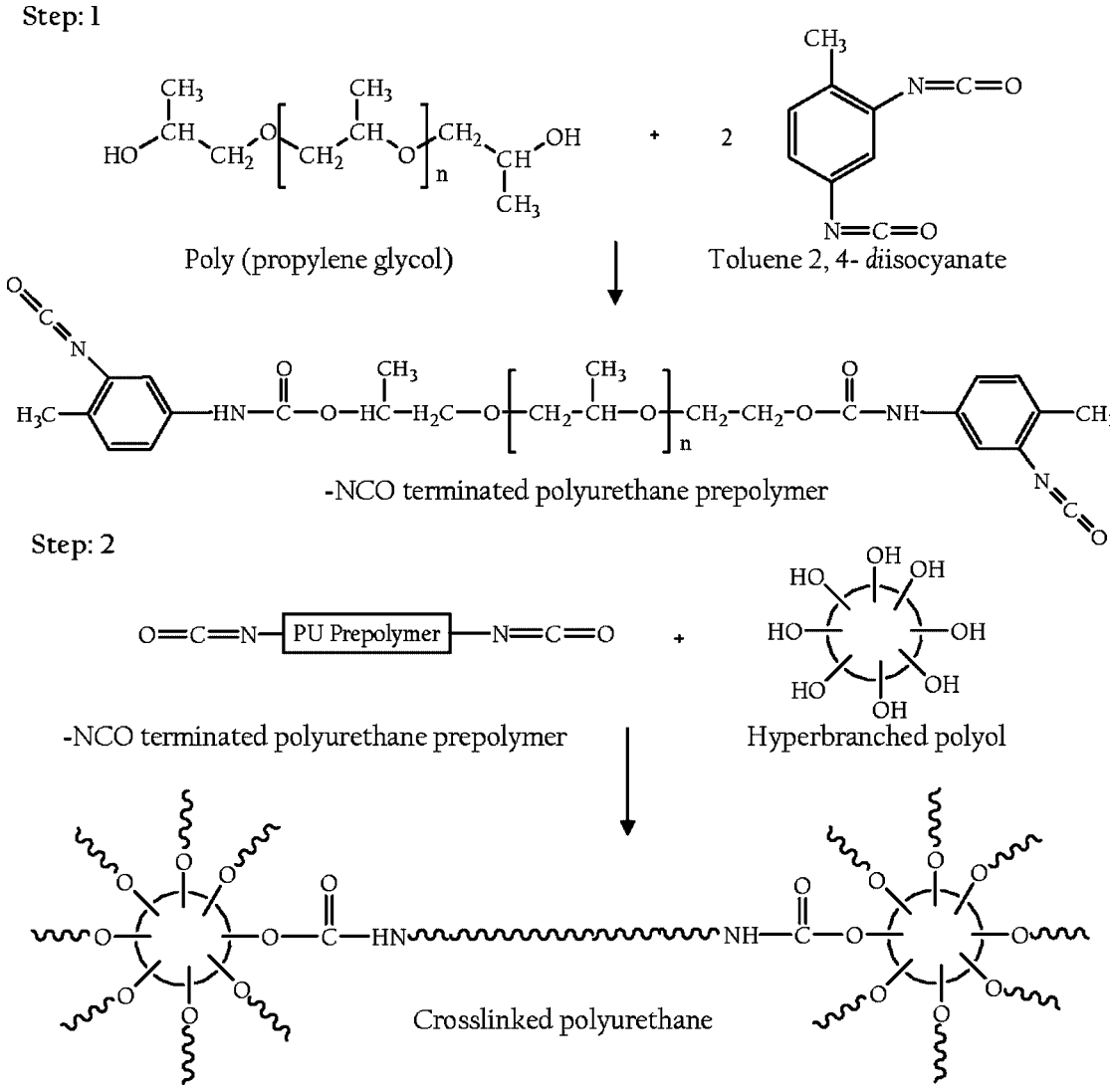

(1984) was found to be 2480 P. The molecular weight determined by the gel permeation chromatography (GPC) method was 2200 g/mol. The PU prepolymer was further characterized by Fourier transform infrared (FTIR) spectroscopy. Proper precautions were taken during the handling of TDI because of its toxicity.

Synthesis of Nanocomposites. For the preparation of the nanocomposite, the prepolymer was reacted with three types of hyperbranched polyol materials (H20, H30, and H40) separately. An equivalent amount of branched polyol was added (equivalent ratio of −NCO:−OH = 1:1) to the diluted prepolymer in THF with constant stirring at room temperature (25 °C) in the presence of 0.001 mol of a DBTL catalyst. In order to investigate the effect of clay on the mechanical and thermal properties and the microstructure of the PU/clay nanocomposite, four concentrations of clay were used: 2.0, 4.0, 8.0, and 16.0 wt %. The clay was dispersed first in THF in a beaker by an ultrasonicator and finally added to the matrix with constant stirring. The samples for mechanical and thermal properties were prepared by casting of the solution in a circular quartz mold, and the thickness was adjusted by the amount of the cast solution. Pure PU was also synthesized by the same procedure without the addition of clay.

CHARACTERIZATION

FTIR Spectroscopic Studies. FTIR studies were carried out in dispersive mode on thin film samples (∼100 μm) using a Perkin-Elmer FTIR spectrophotometer (model spectrum RX I), within a range of 400−4400 cm^{-1} using a resolution of 4 cm^{-1}. An average of 16 scans was reported for each sample.

X-ray Diffraction (XRD) Studies. The XRD patterns of the samples were recorded in a Philips X-ray diffractometer (model PW-1710) at crystal monochromated Co Kα radiation in the angular range 2−10° (2θ) at 40 kV operating voltage and 20 mA current.

Transmission Electron Microscopy (TEM). The samples for TEM analysis were prepared by ultracryomicrotomy with a Leica Ultracut UCT (Leica Mikrosystems GmbH, Vienna, Austria). Freshly sharpened glass knives with cutting edges of 45° were used to obtain cryosections of 50−70 nm thickness. Because these samples were elastomeric in nature, the sample and glass knife temperatures during ultracryomicrotomy were kept constant at −50 and −60 °C, respectively [these temperatures were well below the glass transition temperatures (T_g's) of PUs]. The cryosections were collected individually in a sucrose solution and directly supported on a copper grid of 300 meshes in size. Microscopy was performed with a JEOL JEM 2010 TEM instrument (Japan), operating at an accelerating voltage of 120 kV.

Dynamic Mechanical Thermal Analysis (DMTA). The DMTA spectra of the samples were obtained by using DMTA of TA Instruments (model 2980 V1.7B). The sample specimens were analyzed in tensile mode at a constant frequency of 1 Hz, a strain of 0.01 %, and a heating rate of 2 °C/min. The data were analyzed by TA Universal analysis software on a TA computer attached to the machine. The storage modulus (E') and loss tangent (tan δ) were measured as a function of the temperature for all of the samples under identical conditions. The temperature corresponding to the peak in the tan δ versus temperature plot was taken as the glass−rubber transition temperature (T_g).

Thermogravimetric Analysis (TGA). TGA was carried out in TA Instruments (model Q50), at a heating rate of 10 °C/min under a nitrogen atmosphere up to 700 °C. The data were analyzed by TA Universal analysis software on a TA computer attached to the machine. A small amount of material (around 5 mg) was used for the TGA study.

Tensile Properties. Tensile specimens were punched out from the cast sheets using ASTM Die-C. The tests were carried out as per the ASTM D 412-98 method in a Universal Testing Machine (Zwick 1445) at a cross-head speed of 500 mm/min at 25 °C. The average of three tests is reported here.

Lap Shear Strength. The lap shear strength between aluminum and aluminum was measured as per the ASTM D 1002-05 method in a Universal Testing Machine (Hounsfield H10KS) at a cross-head speed of 1.3 mm/min. The average of three tests is reported here.

Peel Strength. The peel strength between aluminum and nylon fabric was measured as per ASTM D 903-98 methods in a Universal Testing Machine (Hounsfield- H10KS) at a cross-head speed of 150 mm/min by Universal Testing Machine Hounsfield H10KS. The average of three tests is reported here.

RESULTS AND DISCUSSION

FTIR Spectroscopy. FTIR experiments were performed to determine first the extent of reaction between PPG and TDI for the formation of PU prepolymer and finally the curing reaction. The reaction scheme is shown in Scheme 1. The isocyanate-terminated PU prepolymer is characterized by a characteristic absorption peak at 2270 cm^{-1}. Figure 2a shows the FTIR spectra of PPG, TDI, and the PU prepolymer. The peaks at 1730 and 3320 cm^{-1} also confirm the development of the PU backbone in the PU prepolymer. The isocyanate absorption peak of the PU prepolymer steadily decreases as the curing proceeds.

The possibility of urethane linkage formation between $-CH_2CH_2OH$ functionalities of the modifiers/structural −OH in clay and −NCO end groups of polymer chains has been investigated by monitoring the stretching frequency of −NCO groups at 2270 cm^{-1} in the FTIR spectrum. For this purpose, 5 g of prepolymer and 0.4 g of dried clay were mixed in the presence of 20 mL of dry THF by a magnetic stirrer at room temperature (25 °C) to produce a uniform mixture for about 2 h. A few drops of the prepolymer/clay mixture were taken in KBr disks and allowed to evaporate from THF for a period of 30 min. The FTIR spectrum of clay is presented in Figure 2b. The structural −OH stretching peak (e.g., from the Al−OH bond) at 3620 cm^{-1}, the $-CH_2CH_2OH$ peak at 3400 cm^{-1}, and the hydrogen-bonded water bending peak at 1630 cm^{-1} (43) are the main interest because both −OH and water are capable of reacting with −NCO groups. Also note that clay exhibits −CH stretching peaks at 2940 and 2860 cm^{-1}, which correspond to hydrocarbon chains of the organic ammonium ions present in treated clays. The clay/polymer reaction was followed by monitoring of the stretching of −NCO and C═O groups. A reduction of −NCO peaks can be due to reactions with structural −OH and $-CH_2CH_2OH$ groups in clay. It is worth noting that the organic ammonium ions, e.g., those present in clays, can potentially promote trimerization of −NCO groups (44); however, this is not observed in the present study because the characteristic peaks at 1695−1715 cm^{-1} due to trimers of −NCO (45) do not appear during the course of the reactions. −NCO peaks did not disappear completely in a period of 120 min. An increase in the area under the carbonyl peak (CO) at 1730 cm^{-1} indicates that the reactions between −NCO and $-CH_2CH_2OH$/structural −OH groups yield urethane linkages. The clay particles in nanocomposites exhibit characteristic bands associated with the stretching of Si−O (1018 cm^{-1}) and Si−O−Al (525 cm^{-1}) and bending of Si−O−Si at 465 cm^{-1}, as shown in Figure 2b.

The same procedure has been applied for a HBP with the nanoclay. However, there is no significant change in the peaks in Figure 2b, indicating that insignificant interaction has taken place between the clay and the hyperbranched materials.

Figure 2c shows the IR spectra of clay (Cloisite 30B), representative pristine PU ($PU_{40}C_0$), and a representative hyperbranched PU/clay nanocomposite ($PU_{40}C_8$). The characteristic peaks of PU and PU nanocomposites are tabulated

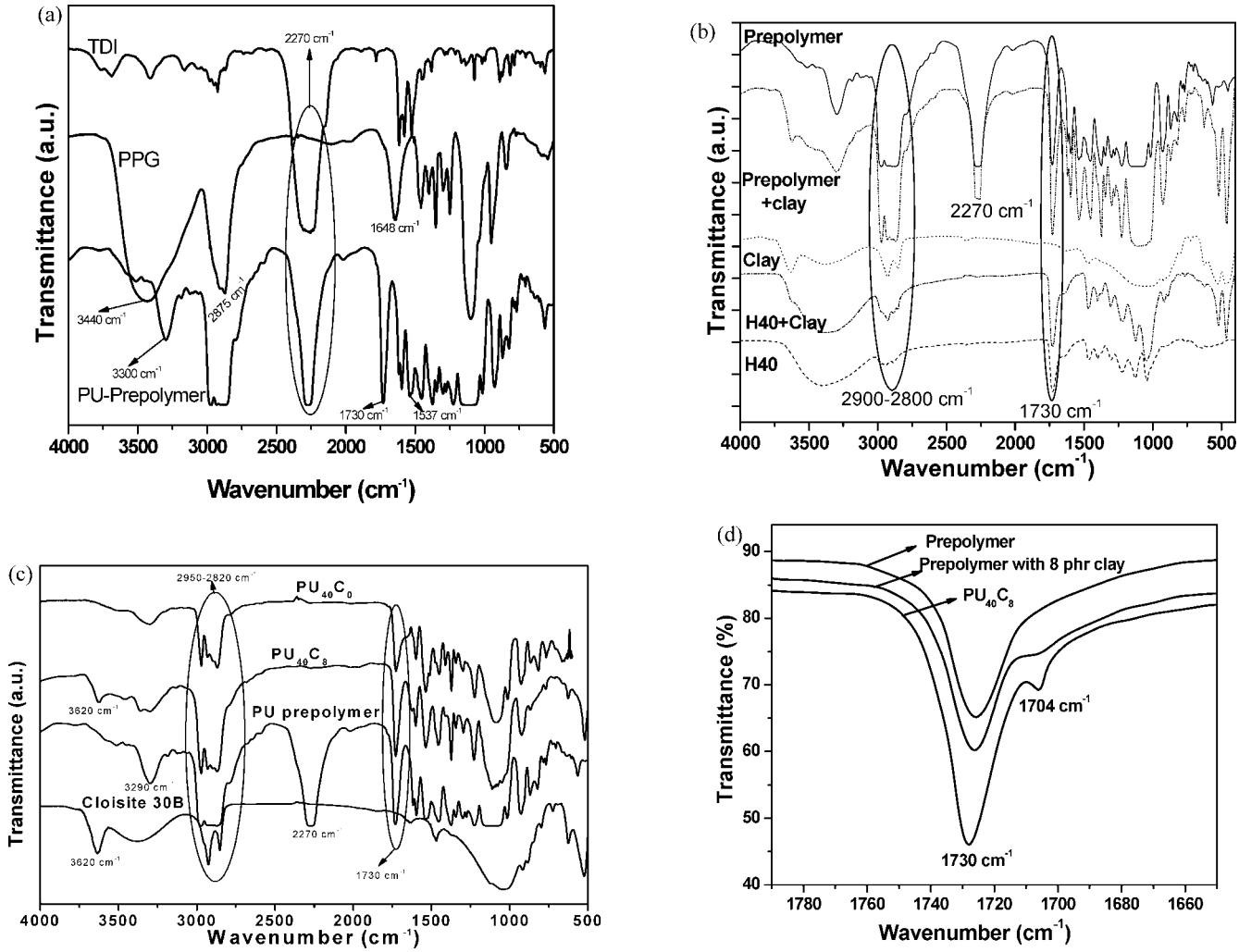

FIGURE 2. (a) FTIR spectra of the TDI, PPG, and the PU prepolymer. (b) FTIR spectra of prepolymer, prepolymer with clay, clay, and clay with fourth-generation HBP, and fourth-generation HBP. (c) FTIR spectra of the clay, PU prepolymer, PU nanocomposite, and pristine PU. (d) FTIR spectra of the enlarged carbonyl peak of the PU prepolymer, prepolymer with clay, and $PU_{40}C_8$.

Table 2. Principal Peak Assignments in the FTIR Spectra of the Pristine PU, PU Prepolymer, PU_{40} C_0, and PU_{40} C_8

obsd peaks (cm^{-1})	peak assignments
3630−3100	NH/−OH stretching vibration
2970−2870	−CH stretching vibration
2270	−NCO stretching vibration
1730	free C═O (urethane) stretching vibration
1704	hydrogen-bonded C═O (urethane) stretching vibration
1620	−NH stretching vibration
1460	$-CH_2$ scissoring vibration
1370−1350	symmetric −CH stretching vibration of $-CH_3$
1250	asymmetric C−O−C stretching vibration
1018	symmetric C−O−C stretching vibration
525	stretching vibration of Si−O−Si
465	Si−O−Al stretching vibration

in Table 2. From Figure 2c, it is clear that the curing process of the PU prepolymer with different hyperbranched polyols is completed because there is no absorption peak at 2270 cm^{-1}. Both pristine PU and PU nanocomposites have characteristic bands at 3325, 2968, 2849, 1730, 1525, 1370, and 1216 cm^{-1}. The 3285 and 3363 cm^{-1} peaks in the FTIR spectra are due to −NH bonding and free −NH groups, respectively. The formation of the urethane C═O group can be determined by examining the peak intensity at 1730 cm^{-1}. Besides these bands, PU nanocomposites have the characteristic bands of MMT at 1018, 525, and 465 cm^{-1} corresponding to the stretching vibration of Si−O, the stretching vibration of Si−O−Al, and the bending vibration of Si−O−Si, respectively. This indicates that the polymer chains have intercalated in the gallery of the MMT clay. In the PU nanocomposites, it is found that the positions of the peaks for the distinctive functional groups are identical with those of the pristine PU, which means that the segmented structure of PU has not been affected by the presence of the clay.

Figure 2d highlights the enlarged carbonyl peaks of the PU prepolymer, prepolymer with 8 parts of clay, and $PU_{40}C_8$. The peak at 1730 cm^{-1} corresponds to the free carbonyl group of the urethane linkage, and the peak at 1704 cm^{-1} indicates the hydrogen-bonded carbonyl groups in the urethane linkage. No peak at 1704 cm^{-1} in the PU prepolymer confirms the absence of hydrogen bonding with the carbonyl

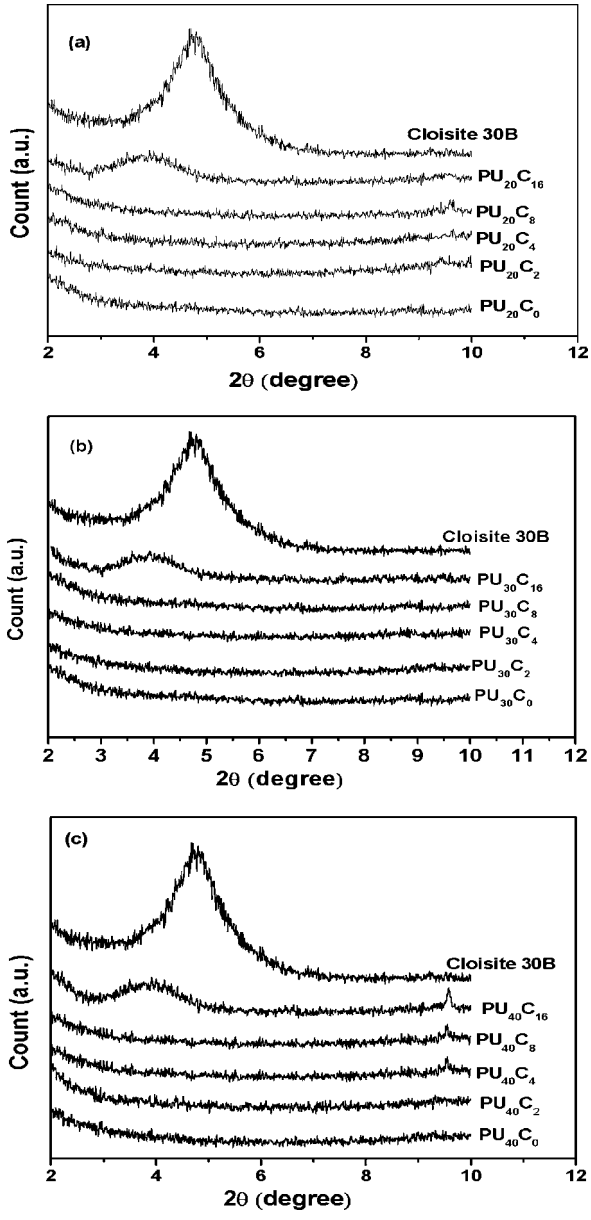

FIGURE 3. XRD patterns of different nanocomposites having different clay loadings: (a) PU_{20}; (b) PU_{30}; (c) PU_{40}.

group. A small peak at 1704 cm^{-1} in the PU prepolymer with clay indicates the tendency to form the hydrogen bond. The peak at 1704 cm^{-1} appears prominent for $PU_{40}C_8$. In the presence of hyperbranched polyol, which has a huge number of hydroxyl −OH groups, a good amount of hydrogen bonding with the C═O group is possible.The urethane linkages can also form hydrogen bonds with the $-CH_2CH_2OH$ group of the modifier of the clay. Because of the lower concentration of the $-CH_2CH_2OH$ group, the hydrogen-bonded carbonyl peak intensity is very low.

Morphology. Wide-angle X-ray scattering (WAXS) spectra have been recorded for the measurement of dispersion of clay in the PU matrix. Parts a−c of Figure 3 show the WAXS spectra for different nanocomposites at various clay loadings. A strong peak at $2\theta = 4.74°$ is observed, corresponding to a basal spacing $d_{001} = 1.85$ nm in the as-received Cloisite 30B. It is no longer visible in PU nanocomposites at Cloisite 30B loading below 8 wt %. Only at higher loading (∼16 wt %) does a peak appear at 3.88° (Figure 3c) for PU_{40}. The organically modified MMT clay undergoes significant expansion at 16 wt % clay content. d_{001} increases from 1.8 to 2.4 nm in the presence of a fourth-generation hyperbranched polyol. An increase in the interlayer spacing is usually indicative of an intercalated structure and the absence of a peak in the XRD pattern indicates the total delamination or exfoliation of nanoclay in the polymer matrix. A similar behavior is observed for the second- and third-generation hyperbranched PU/clay nanocomposites (Figure 3a,b).

A key factor in the effectiveness of hyperbranched polyols in delamination of Cloisite 30B clay is thought to be their high degree of end-group functionality and high tethering densities of linear end-functional chains. This is reflected in the properties of the PU nanocomposites, which are discussed in subsequent sections.

The efficiency of exfoliation and good dispersion of clay are also demonstrated by TEM. Some representative micrographs are given in Figures 4 and 5. Figure 4 shows the TEM morphology of the PU nanocomposites having 2, 4, 8, and 16 wt % organoclay loading of PU_{40}. The dark lines represent individual clay layers, whereas the bright area is for the polymer matrix. The photography shows a homogeneous dispersion of silicate layers in the polymer matrix up to 8 phr clay loading (Figure 4c). These also indicate partial intercalation and exfoliation of the silicate layers. Dispersion of organoclays in the PU matrix depends on the nature of the organoclays and especially the polar interaction between the silicate layers and the PU prepolymer/hydroxyl-functionalized HBPs. This is greatly improved because of the strong hydrogen-bonding interaction between the hydroxyl groups of silicate layers and those of the HBPs (Figure 2d). Figure 4d exhibits the morphology of $PU_{40}C_{16}$ filled with 16 phr of organoclay loading. The image shows intercalation of silicate layers throughout the PU matrix instead of exfoliation. These results are in agreement with the XRD results as shown earlier. Morphology of the other systems based on PU_{20} and PU_{30} follows the same trend as shown that above. Figure 5 shows representative photographs of nanocomposites of PU_{20} and PU_{30}. It is shown that good dispersion of the clay layer takes place up to 8 phr of clay loading.

The results from XRD and TEM show that silicate layers are exfoliated when the content of layer silicate in the PU matrix is lower (up to 8 wt %), whereas agglomeration of clay particles takes place in the matrix when the weight fraction increases.

DMTA. The dissipation factor (tan δ) and storage modulus (E') curves are presented in Figures 6 and 7 for the representative samples. The details are given in Table S1 in the Supporting Information. The tan δ peak is associated with the glass transition temperature (T_g) of the soft segment. The hard segment T_g is often difficult to detect in this type of PU (46), and it is not clearly observed for any of the materials studied here. T_g is observed to increase in an approximately linear fashion with the increased addition of

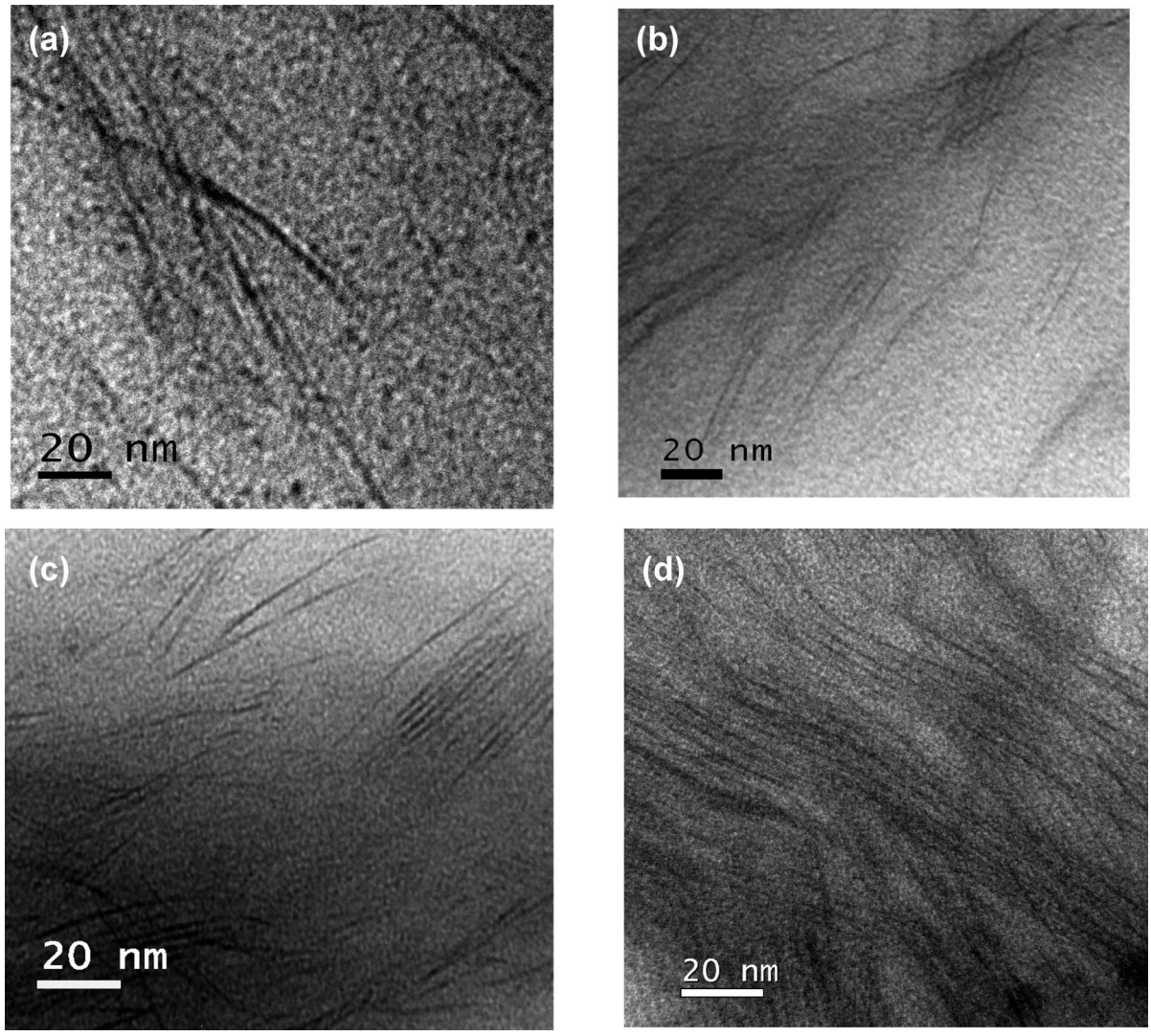

FIGURE 4. TEM photographs of different PUs at various clay loadings: (a) $PU_{40}C_2$; (b) $PU_{40}C_4$; (c) $PU_{40}C_8$; (d) PU_8C_{16}.

clay particles (Figure 6a,b). The results are in agreement with those reported by Maiti and Bhowmick (47) in the fluoroelastomer nanocomposites. For example, T_g for the neat PU ($PU_{40}C_0$) is −20 °C, whereas the same for the nanocomposite having 8 wt % loading of clay is −14 °C. An approximately 6 °C shift is observed with 8 wt % clay loading. The magnitude of the tan δ peak also decreases with an increase in the concentration of clay, shown in the same figure. Mishra et al. (48) and Xiong et al. (49) reported the same trend for the linear PU nanocomposites. The tan δ peak for $PU_{40}C_0$ is observed at 0.60, which reduces to 0.44 for $PU_{40}C_8$. This is mainly attributed to good adhesion between the PU and the clay particles, as a result of which the nanometer-sized particles can restrict the segmental motion near the organic−inorganic interface. This is applicable for all of the PUs. Another interesting phenomenon observed here is that with an increase in the functionality of the hyperbranched polyol, more efficient anchoring takes place as a result of the presence of a higher number of hydroxyl groups. Obviously, higher T_g (−20 °C) is observed for $PU_{40}C_0$ as compared to those of $PU_{30}C_0$ and $PU_{20}C_0$ (−22 and −24 °C, respectively). This is in good agreement with the theoretical prediction for highly branched polymers and is analogous to the results on linear polymers (50); i.e., longer arms yield higher glass relaxation temperatures.

It is apparent that the addition of clay platelets leads to an increase in the storage modulus consistent with the reinforcing action of the addition of the clay as a filler (Figure 7). The storage modulus increases with the addition of clay. For example, $PU_{40}C_0$ has a logarithmic modulus value of 0.84 MPa, which is increased to 1.19 MPa with the addition of 8% of clay at 25 °C. Ma et al. (51) show the same trend of an increase of the storage modulus in rectorite/linear thermoplastic PU nanocomposites. A higher storage modulus is observed for the case of fourth-generation hyperbranched PU. As the temperature increases, the nanocomposites show a gradual drop in the storage modulus, as usual. The dynamic mechanical properties at selected temperatures are reported in Table S1 in the Supporting Information. The storage modulus of the nanocomposite film at 8 wt % loading at 25 °C is increased by 194%, 89%, and 51% over the pristine material of PU_{20}, PU_{30}, and PU_{40} respectively. The enhancement is lower at higher concentration and can be attributed to intercalation and agglomeration of clay. Our

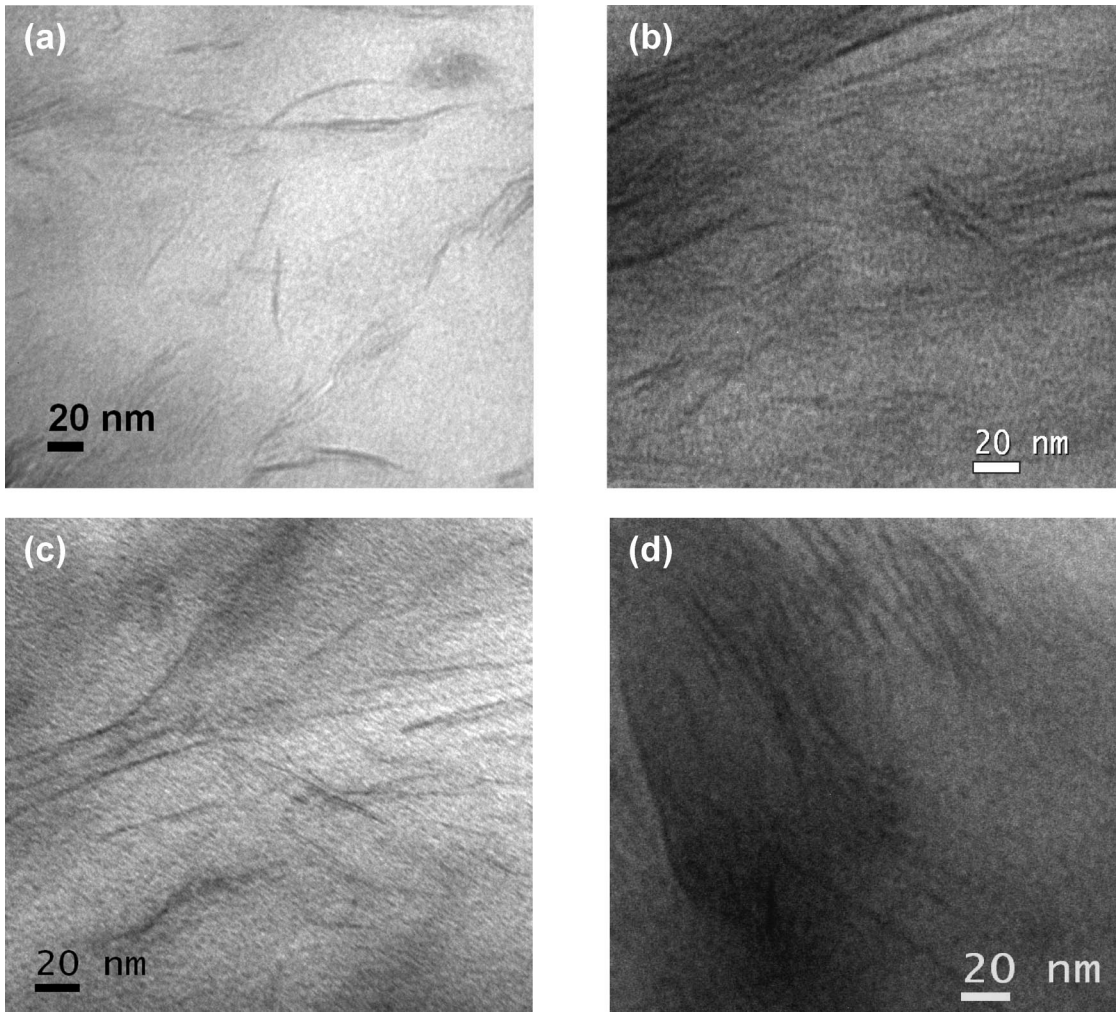

FIGURE 5. TEM photographs of different PUs at various clay loadings: (a) $PU_{20}C_2$; (b) $PU_{20}C_8$; (c) $PU_{30}C_4$; (d) $PU_{30}C_8$.

study also shows that the molecular weight of the hyperbranched polyester can have a significant effect on the viscoelastic properties of the cured PUs. The T_g and storage modulus values move toward higher temperature as the molecular weight and also the functionality increase.

Thermal Properties. Thermal stability of pristine PU and its nanocomposites having different clay loadings has been investigated by TGA. The degradation behavior of the representative nanocomposites is shown in Figure 8a,b. The data obtained from these curves are given in Table S2 in the Supporting Information, which shows the quantitative values of the onset degradation temperature, the temperature at which the maximum degradation takes place (T_{max}), and the rate of degradation for various PU nanocomposites. A gradual weight loss is observed starting at around 320 °C for all of the PUs. This initial weight loss is possibly due to the degradation of the hard segment present in the PU matrix, which continues for some period at a very slow rate. Because the actual decomposition of the cured nanocomposites begins at elevated temperatures, the weight loss occurs at a faster rate. The intersection point between the initial slope and the slope followed after the fast decomposition basically provides primary onset of the decomposition temperature (T_i). T_i values are directly computed by the TGA instrument. The samples containing nanoclay particles provide a higher T_i than the pristine PU. With an increase of the clay loading, T_i increases. From the differential thermogravimetry data shown in the inset of Figure 8a,b, T_{max} increases from 380 to 388 °C, from 383 to 394 °C, and from 402 to 410 °C for PU_{20}, PU_{30}, and PU_{40}, respectively, from their pristine PU at 16 parts of clay loading. The degradation rate of the nanocomposites also decreases with an increase of the clay loading. This indicates an improvement of the thermal stability of the PUs with the addition of clay. This is due to the fact that the inorganic material can prevent heat and limit further degradation. A similar result of thermal stability has also been reported for polypropylene/clay (52), polyimide/clay (53), and polystyrene/clay (54). With an increase of the functionality of the polyol, the thermal stability of the PU increases. This increase in the thermal stability with an increase of generation of polyol could be due to increasing cross-linking owing to the availability of a higher number of end hydroxyl functional groups that take part in the cross-linking reaction.

Tensile Properties. Parts a and b of Figure 9 show tensile properties of representative nanocomposites. The data calculated from the plots are given in Table S3 in the Supporting Information. The modulus increases in general

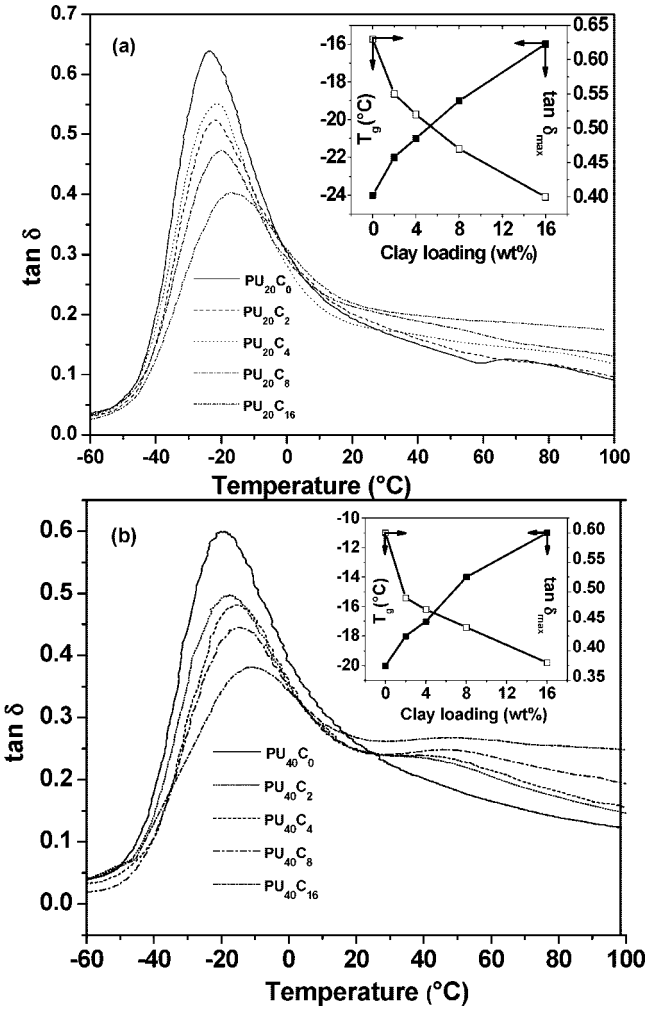

FIGURE 6. tan δ vs temperature plots for different PU nanocomposites: (a) PU_{20}; (b) PU_{40}.

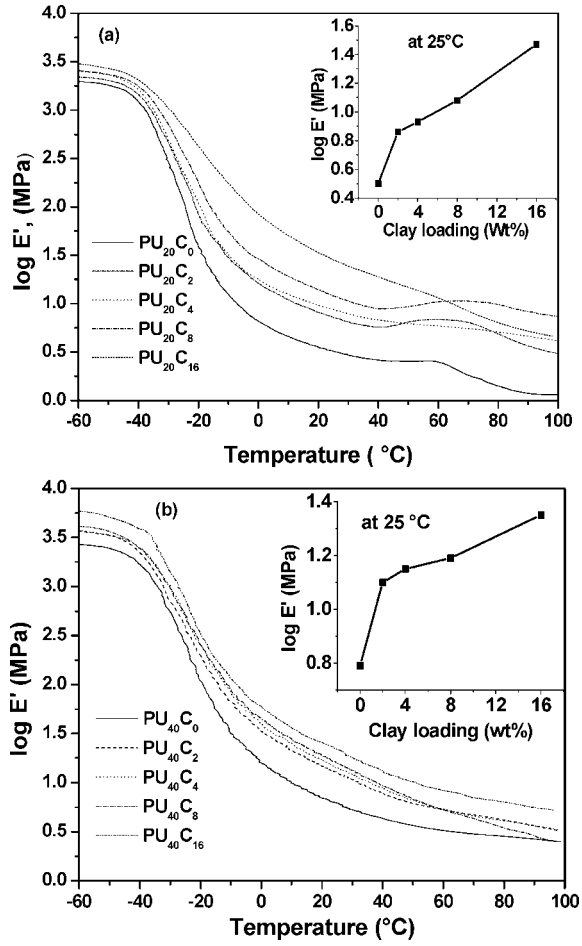

FIGURE 7. Storage modulus δ vs temperature plots for different PU nanocomposites: (a) PU_{20}; (b) PU_{40}.

with the loading of clay. There is a 73% increase of 100% modulus with the addition of 8 phr of clay in PU_{20}. The ratio of the modulus E_0/E_m at 100% elongation is shown in the inset of Figure 9a,b, where E_0 is the modulus value of the nanocomposites and E_m is the modulus of the pristine PU. It is interesting to note that all of the PUs behave exactly the same way, independent of hydroxyl number of the branched materials. The modulus initially increases sharply with clay loading up to 8 phr, beyond which the increase is less. The tensile strength increases gradually up to 8 wt % clay loading before a decrease at higher loading. From XRD and TEM investigations in the previous section, it is observed that good dispersion and exfoliation is achieved up to 8 wt % clay loading. The homogeneous dispersion of individual layers shows an effective reinforcement effect for the polymer matrix. The nanodispersed clay with a high aspect ratio provides a higher stress-bearing capability and efficiency. Stronger interactions between nanoclay layers and the polymer molecules (FTIR analysis in the previous section) associated with a larger contact surface result in effective constraint of the motion of the polymer chains. It is believed that the presence of more polar groups and ionic interaction between polymer chains and silicate layers increase the tensile strength of the nanocomposites. Hydroxyl-terminated HBP facilitates the interaction between the polymer and silicate layers. Above 8 wt % organoclay loading, the formation of a homogeneous nanostructure filler is more difficult. The organoclay layers are found in the form of agglomeration in the PU matrix, as shown in the XRD and TEM investigations. Because of the agglomeration of the nanofillers, the filler−filler interaction is predominant over the filler−polymer interaction. Also, agglomerated particles act as defects. As a result, a decrease in the tensile strength is observed in all of the nanocomposites containing 16 wt % clay loading. Figure 10 shows the effect of the number of functionalities of branched polyols and clay loading on the tensile strength of different PU nanocomposites. There are 135%, 138%, and 106% increases in the tensile strength over the pristine PU in the cases of PU_{20}, PU_{30}, and PU_{40}, respectively, at 8 phr of clay loading. Song et al. (55) reported the same trend of an increase in the tensile strength of linear PU nanocomposites with clay loading. However, the values are much lower than those of the nanocomposites reported here. The superior tensile properties are attributed to the higher number of end −OH functionalities in the branched cross-linker molecules. The addition of nanofillers has a synergistic effect on the tensile properties of the PUs. With the addition of nanoclays, even the elongation at break of the PU nanocomposites increases. The elongation at break increases by 32%, 58%, and 85% for PU_{20}, PU_{30}, and PU_{40},

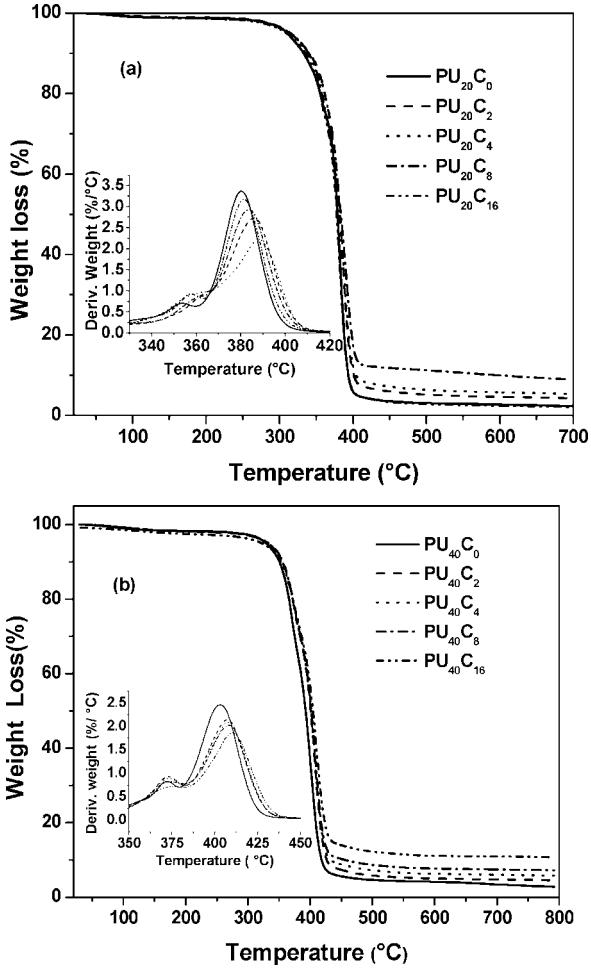

FIGURE 8. TGA thermogram of PU nanocomposites: (a) PU_{20}; (b) PU_{40}.

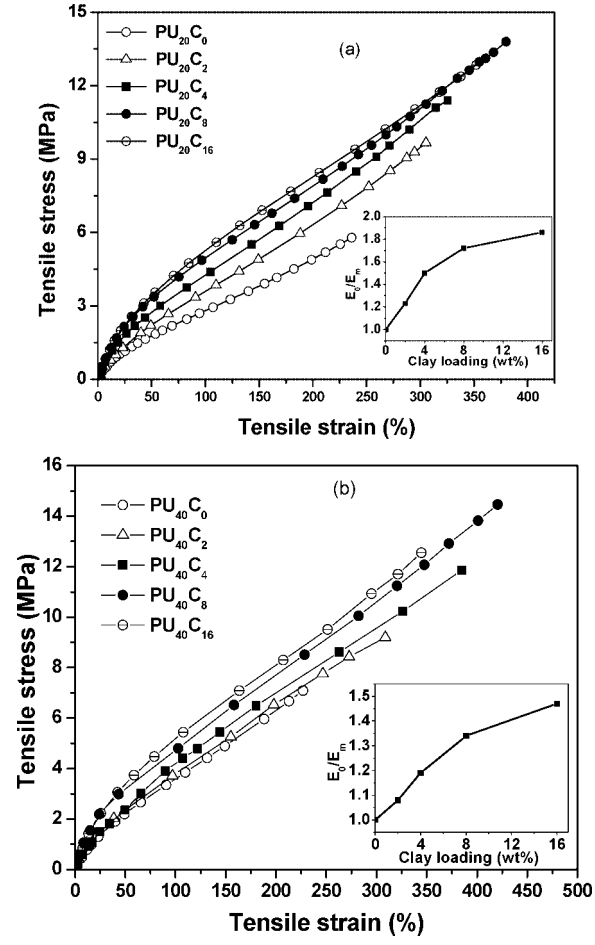

FIGURE 9. Tensile properties of PU samples having different clay loadings: (a) PU_{20}; (b) PU_{40}.

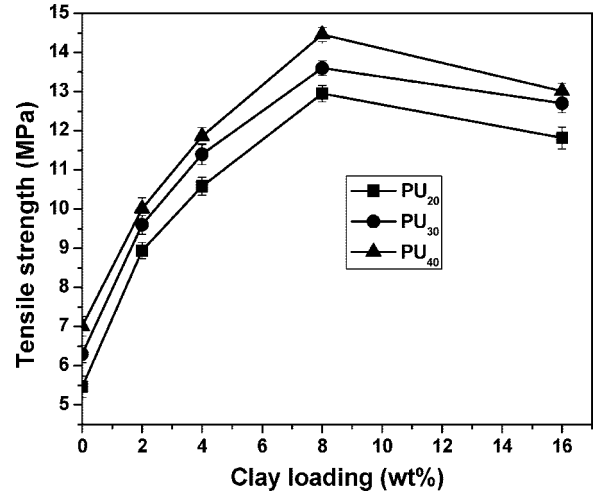

FIGURE 10. Variation of the tensile strength of the different PUs having different clay loadings.

respectively, over their pristine PUs at 8 phr clay loading. The increase in the elongation at break is mainly due to the plasticization effect of the nanoclays in the PU matrix and also due to the enhanced stress-bearing capability of the nanocomposites. It is interesting to note that with an increase in the functionality in the hyperbranched polyol, the tensile strength increases in the pristine PUs.

Adhesive Properties. The effect of the clay content in the PU on the lap shear strength between aluminum and aluminum is shown in Figure 11a. Incorporation of clay into the PU matrix results in an improvement of the joint strength in all of the cases up to a certain loading. The addition of 8 wt % clay in the case of PU_{40} leads to about a 2-fold increase in the lap shear strength over the pristine PU. The 180° peel strength of the Al plate to nylon fabric by using PU nanocomposite as an adhesive is given in Figure 11b. With the addition of 8 wt % clay into the PU matrix of PU_{40}, the 180° peel strength is increased about 200% over the neat PU sample. Patel et al. (56) reported the same trend of an increase in the peel strength with the addition of nanoclay as an acrylic adhesive. It is also interesting that the HBP having a higher level of functionality imparts higher lap shear and peel strengths. van der Waals interaction, adsorption, and increased strength with 8 wt % clay loading give rise to enhanced adhesive strength. Above 8 wt % clay loading, aggregation and reduced strength play major roles in the lowering of adhesion.

CONCLUSIONS

Syntheses involving reactive hyperbranched polyols and PU prepolymer and their nanocomposites yield a thermally stable and mechanically strong clay PU nanocomposite. The dispersion of nanoparticles was charac-

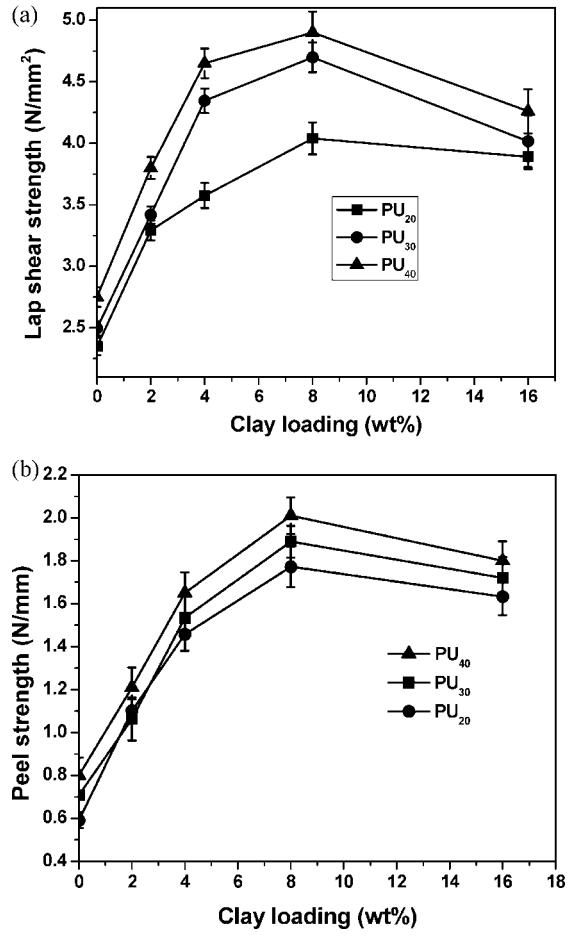

FIGURE 11. (a) Lap shear strength between aluminum and aluminum with PU adhesive having different clay loadings. (b) Peel strength between aluminum and nylon fabric with PU adhesive having different clay loadings.

terized by XRD and TEM, showing that clay was homogeneously dispersed and exfoliated in the PU matrix at a low content of clay (less than 8%). At higher content, agglomeration of clays resulted in nonuniform dispersion. The cured nanocomposites exhibited excellent mechanical and adhesive properties and thermal stability compared to pristine PU. The nanocomposite containing 8 wt % clay loading showed a ~100% increase in the tensile strength, a ~2-fold increase in the lap shear strength, and a ~200% increase in the peel strength, along with dramatic improvement in thermal and dynamic mechanical thermal properties over the control PU. The addition of the organoclay significantly increased the moduli of the materials above and below T_g.

Acknowledgment. The financial support of this work by Indian Space Research Organization is gratefully acknowledged.

Supporting Information Available: Tables showing data of dynamic mechanical properties at various temperatures, thermogravimetry, and tensile properties of various PU nanocomposites. This material is available free of charge via the Internet at http://pubs.acs.org.

REFERENCES AND NOTES

(1) Xu, R.; Manias, E.; Snyder, A. J.; Runt, J. *J. Biomed. Mater Res.* **2003**, *64*, 114.
(2) Hu, Y.; Wang, S.; Ling, Z.; Zhuang, Y. L.; Chen, Z.; Fan, W. C. *Macromol. Mater. Eng.* **2003**, *288*, 272.
(3) Zhang, J.; Manias, E.; Wilkie, C. A. *J. Nanosci. Nanotechnol.* **2008**, *8*, 1597.
(4) Rao, Y.; Blanton, T. N. *Macromolecules* **2008**, *41*, 935.
(5) Giannelis, E. P. *Adv. Mater.* **1996**, *8*, 29.
(6) Tamura, K.; Yokoyama, S.; Pascua, C. S.; Yamada, H. *Chem. Mater.* **2008**, *20*, 2242.
(7) Yoo, Y.; Paul, D. R. *Polymer* **2008**, *49*, 3795.
(8) Chavarria, F.; Nairn, K.; White, P.; Hill, A. J.; Hunter, D. L.; Paul, D. R. *J. Appl. Polym. Sci.* **2007**, *105*, 2910.
(9) Chigwada, G.; Wang, D.; Jiang, D. D.; Wilkie, C. A. *Polym. Degrad. Stab.* **2006**, *91*, 755.
(10) Ghosh, A. K.; Woo, E. M. *Polymer* **2004**, *45*, 4749.
(11) Xue, S.; Pinnavaia, T. J. *Microporous Mesoporous Mater.* **2008**, *107*, 134.
(12) Ngo, T. D.; Ton-That, M. T.; Hoa, S. V.; Cole, K. C. *J. Appl. Polym. Sci.* **2008**, *107*, 1154.
(13) Solar, L.; Nohales, A.; Muñoz-Espí, R.; López, D.; Gómez, C. M. *J. Polym. Sci., Part B: Polym. Phys.* **2008**, *46*, 1837.
(14) Langat, J.; Bellayer, S.; Hudrlik, P.; Hudrlik, A.; Maupin, P. H.; Gilman, J. W. *Polymer* **2006**, *47*, 6698.
(15) Campbell, S.; Liang, M. I. *High Perform. Polym.* **2006**, *18*, 71.
(16) Tyan, H. L.; Leu, C. M.; Wei, K. H. *Chem. Mater.* **2001**, *13*, 222.
(17) Maiti, M.; Bhowmick, A. K. *J. Polym. Sci., Part B: Polym. Phys.* **2006**, *44*, 162.
(18) Ganguly, A.; Sarkar, M. D.; Bhowmick, A. K. *J. Appl. Polym. Sci.* **2006**, *100*, 2040.
(19) Sadhu, S.; Bhowmick, A. K. *J. Appl. Polym. Sci.* **2004**, *92*, 698.
(20) Cui, L.; Tarte, N. H.; Woo, S. I. *Macromolecules* **2008**, *41*, 4268.
(21) Chang, C. C.; Hou, S. S. *Eur. Polym. J.* **2008**, *44*, 1337.
(22) Cui, L.; Tarte, H. N.; Woo, S. I. *J. Appl. Polym. Sci.* **2008**, *110*, 784.
(23) Bhowmick, A. K.; Stephens, H. L. *Handbook of Elastomers*, 2nd ed.; Marcel Dekker: New York, **2001**.
(24) Hepburn, C. *Polyurethane Elastomers*; Elsevier Science: New York, **1982**.
(25) Pattanayak, A.; Jana, S. C. *Polymer* **2005**, *46*, 5183.
(26) Pattanayak, A.; Jana, S. C. *Polym. Eng. Sci.* **2005**, *45*, 1532.
(27) Rehab, A.; Akelah, A.; Agag, T.; Shalaby, N. *Polym. Adv. Technol.* **2007**, *18*, 463.
(28) Sadhu, S.; Bhowmick, A. K. *J. Polym. Sci., Part B: Polym. Phys.* **2004**, *42*, 1573.
(29) Sadhu, S.; Bhowmick, A. K. *Rubber Chem. Technol.* **2005**, *78*, 321.
(30) Bandyopadhyay, A.; Maiti, M.; Bhowmick, A. K. *Mater. Sci. Technol.* **2006**, *22*, 818.
(31) Bandyopadhyay, A.; Sarkar, M. D.; Bhowmick, A. K. *Rubber Chem. Technol.* **2005**, *78*, 806.
(32) Ganguly, A.; Sarkar, M. D.; Bhowmick, A. K. *J. Polym. Sci., Part B: Polym. Phys.* **2007**, *45*, 52.
(33) Maiti, M.; Sadhu, S.; Bhowmick, A. K. *J. Polym. Sci., Part B: Polym. Phys.* **2004**, *42*, 4489.
(34) Maiti, M.; Bhowmick, A. K. *Polymer* **2006**, *47*, 6156.
(35) Mariarosaria, T.; Giuliana, G.; Vittoria, V.; Giancarlo, G.; Stefano, R.; Emo, C. *Polymer* **2002**, *43*, 6147.
(36) Ahmed, R.; Nehal, S. *Mater. Sci. Eng. A* **2005**, *399*, 368.
(37) Buhleier, E.; Wehner, W.; Vögtle, F. *Synthesis* **1978**, 155.
(38) Tomalia, D. A.; Barker, H.; Dewald, J. R.; Hall, M.; Kallos, G.; Martin, S.; Roeck, J.; Ryder, J.; Smith, P. *Polym. J.* **1985**, *17*, 117.
(39) Tomalia, D. A.; Barker, H.; Dewald, J. R.; Hall, M.; Kallos, G.; Martin, S.; Roeck, J.; Ryder, J.; Smith, P. *Macromolecules* **1986**, *19*, 2466.
(40) Newkome, G. R.; Yao, Z.-Q.; Baker, G. R.; Gupta, V. K. *J. Org. Chem.* **1985**, *50*, 2003.
(41) Unal, S.; Yilgor, I.; Yilgor, E.; Sheth, J. P.; Wilkes, G. L.; Long, T. E. *Macromolecules* **2004**, *37*, 7081.
(42) Chen, C. P.; Dai, S. A.; Chang, H. L.; Su, W. C.; Wu, T. M.; Jeng, R. J. *Polymer* **2005**, *46*, 11849.
(43) Madejova, J. *Vib. Spectrosc.* **2003**, *31*, 1.
(44) Lin, I. S.; Kresta, J. E.; Frisch, K. C. Reaction injection molding and fast polymerization reactions. *Polymer Science and Technology*; Plenum Press: New York, **1982**; Vol. 18, p 147.
(45) Lyman, D. J. *Rev. Macromol. Chem.* **1966**, *1*, 191.
(46) Tien, Y. I.; Wei, K. H. *J. Appl. Polym. Sci.* **2002**, *86*, 1741.
(47) Maiti, M.; Bhowmick, A. K. *Compos. Sci. Technol.* **2008**, *68*, 1.
(48) Mishra, J. K.; Kim, I.; Ha, C. S. *Macromol. Rapid Commun.* **2003**, *24*, 671.

(49) Xiong, J.; Liu, Y.; Yang, X.; Wang, X. *Polym. Degrad. Stab.* **2004**, *86*, 549.
(50) Asif, A.; Shi, W.; Shen, X.; Nie, K. *Polymer* **2005**, *46*, 11066.
(51) Ma, X.; Lu, H.; Lian, G.; Zhao, J.; Lu, T. *J. Appl. Polym. Sci.* **2005**, *96*, 1165.
(52) Kodgire, P.; Kalgaonkar, R.; Hambir, S.; Bulakh, N.; Jog, J. P. *J. Appl. Polym. Sci.* **2001**, *81*, 1786.
(53) Tyan, H. L.; Wei, K. H.; Hsieh, T. E. *J. Polym. Sci., Part B: Polym. Phys.* **2000**, *38*, 2873.
(54) Fu, X.; Qutubuddin, S. *Polymer* **2001**, *42*, 807.
(55) Song, L.; Hu, Y.; Li, B.; Wang, S.; Fan, W. *Int. J. Polym. Anal. Charact.* **2003**, *8*, 317.
(56) Patel, S.; Bandyopadhyay, A.; Ganguly, A.; Bhowmick, A. K. *J. Adhesion Sci. Technol.* **2006**, *20*, 371.

AM800020K